Supporting Information

Ultrasound-Induced Magnetic Imaging of Tumors Targeted by Biofunctional Magnetic Nanoparticles

Kai-Wen Huang[†,‡], Jen-Jie Chieh[§,*], Chih-KuangYeh[‖] , Shu-Hsien Liao[§], Yi-Yan Lee[§], Pei-Yi Hsiao[§], Wen-Chun Wei[§], Hong-Chang Yang[§], and Herng-Er Horng[§]

[†]Department of Surgery and Hepatitis Research Center, National Taiwan University Hospital, 100Taipei, Taiwan

[‡]Graduate Institute of Clinical Medicine, National Taiwan University, 100 Taipei, Taiwan

[§]Institute of Electro-Optical Science and Technology, National Taiwan Normal University, 116Taipei, Taiwan

[‖]Department of Biomedical Engineering and Environmental Sciences, National Tsing Hua University, 300Hsinchu, Taiwan

[*]Correspondence to J. J. C. (jjchieh@ntnu.edu.tw)

Contents

1. The synthesis of the magnetic reagent

The synthesis process of the utilized magnetic reagent included the synthesis of water-based Fe_3O_4 magnetic fluids and water-based antibody/dextran-coated Fe_3O_4magnetic fluids[S1], as shown in Figure S1. Here, the utilized antibody was alpha-fetoproteinprotein antibody (anti-AFP) (EA502-Q1053, EastCoast Bio, USA).

The MNP sizes were largely controlled in the last step of the gel filtration chromatography, as shown in Figure S1a.The collection time of water-based Fe_3O_4 MNPs in one bottle determined the homogenousness. Although the short collection time resulted in excellent homogenousness, the collected volume was small. Hence, the characteristic reproducibility of utilized anti-AFP MNPs was well controlled.

For example, the utilized magnetic reagents were synthesized from two batches of water-based anti-AFP/dextran-coated Fe_3O_4 MNPs. These two batches showed the similar average hydrodynamic diameters of 57.3 ± 15.2 and 55.5 ± 9.8 nm when measured by a nanoparticle size analyzer (Microtrac, Montgomeryville, PA, USA) as shown in Figure S2. The magnetization-field curves were measured by using a vibrating sample magnetometer (EG&G PARC, Newnan, GA); they showed the superparamagnetic properties and other characteristics illustrated in Figure S3.

Although the particle size and the size distribution of anti-AFP MNPs are able to influence various magnetic characteristics including saturation magnetization[S2], the quantities of test reagents and anti-AFP MNPs were controlled with the same saturation magnetization in this work. Consequently, the saturation magnetization under the ultrasound vibration produced signals that were theoretically the same even though the anti-AFP MNPs were vastly different in size and size distribution.

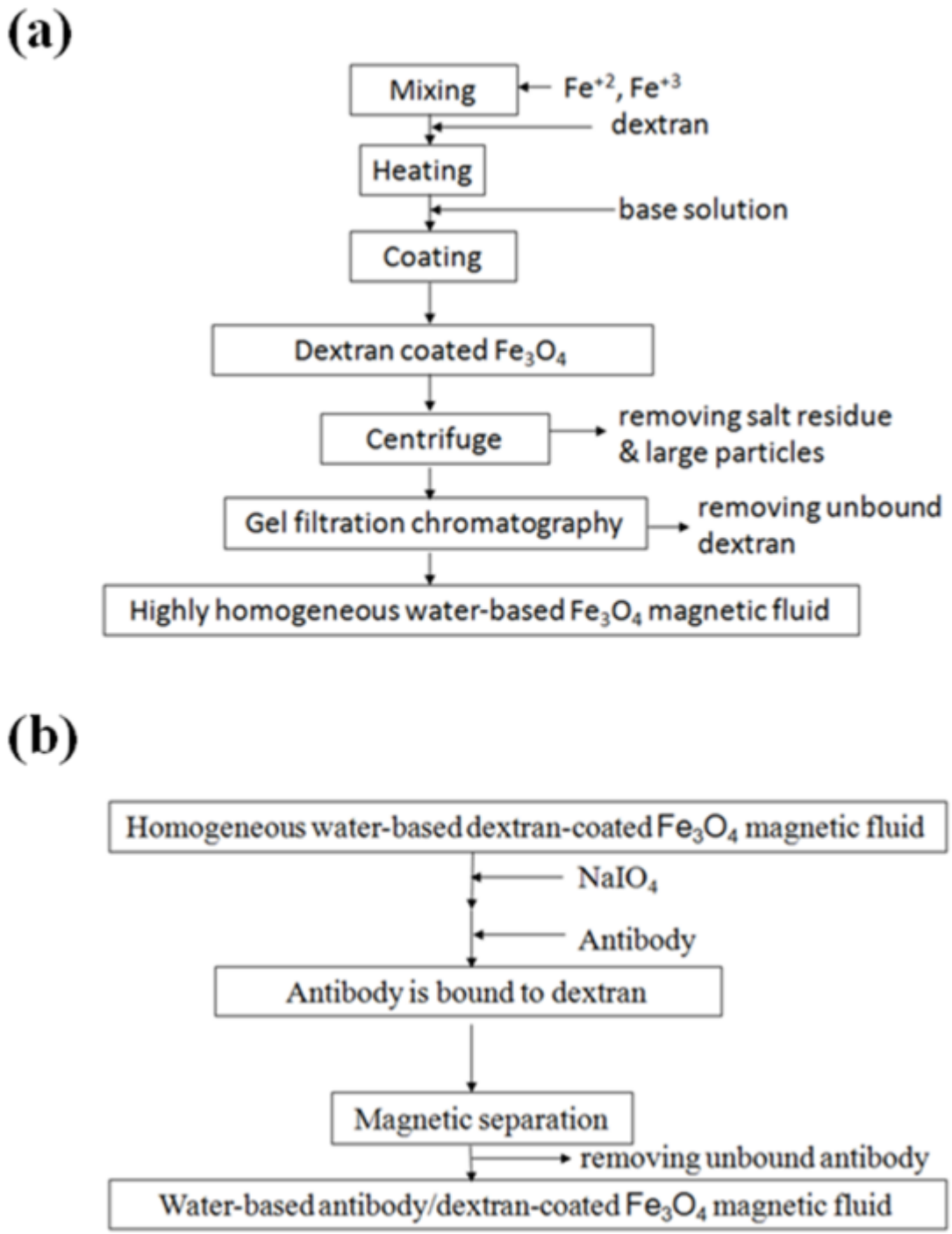

Figure S1. Synthesis process of components of utilized anti-AFP MNPs. (a) water-based Fe_3O_4 MNPs, (b) water-based anti-AFP /dextran-coated Fe_3O_4 magnetic fluid.

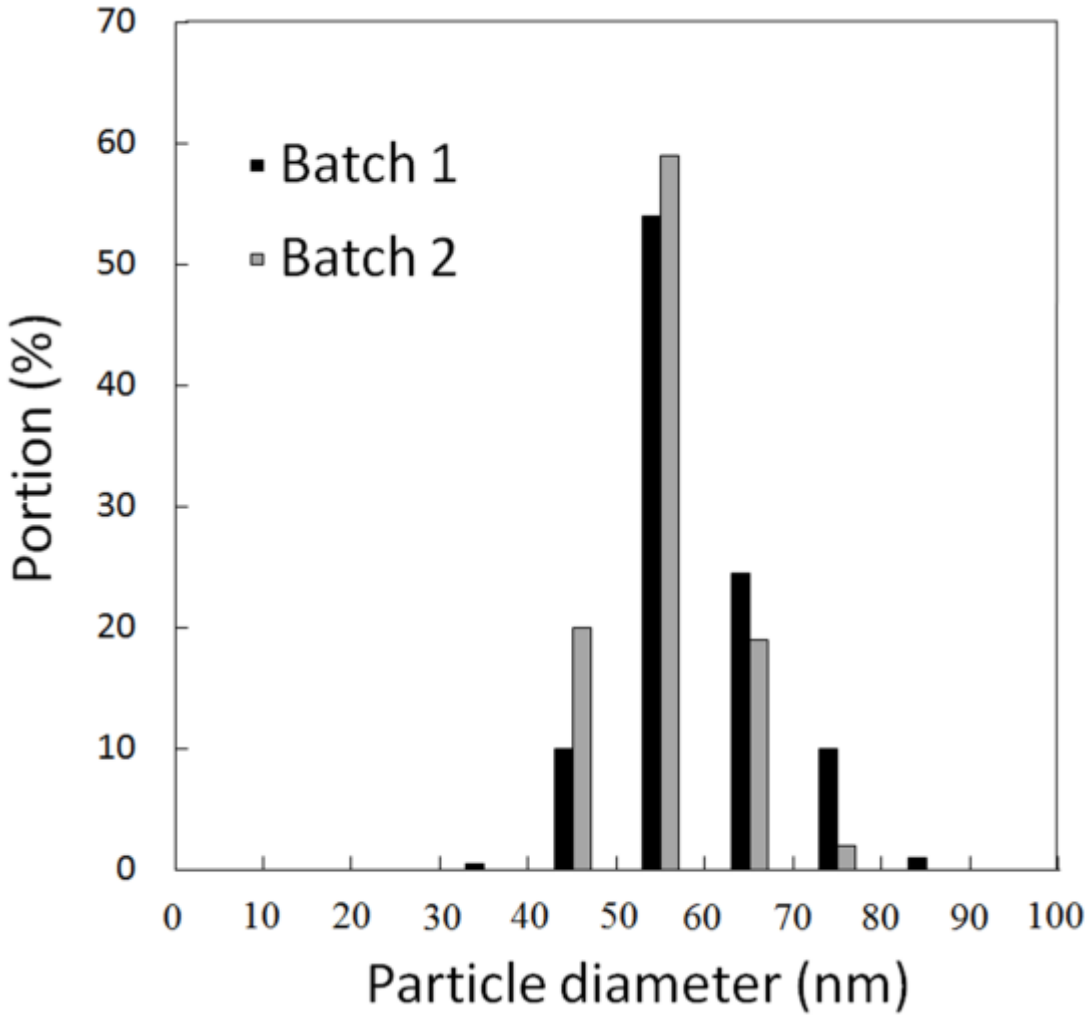

Figure S2. Particle sizes of two batches of anti-AFP reagent

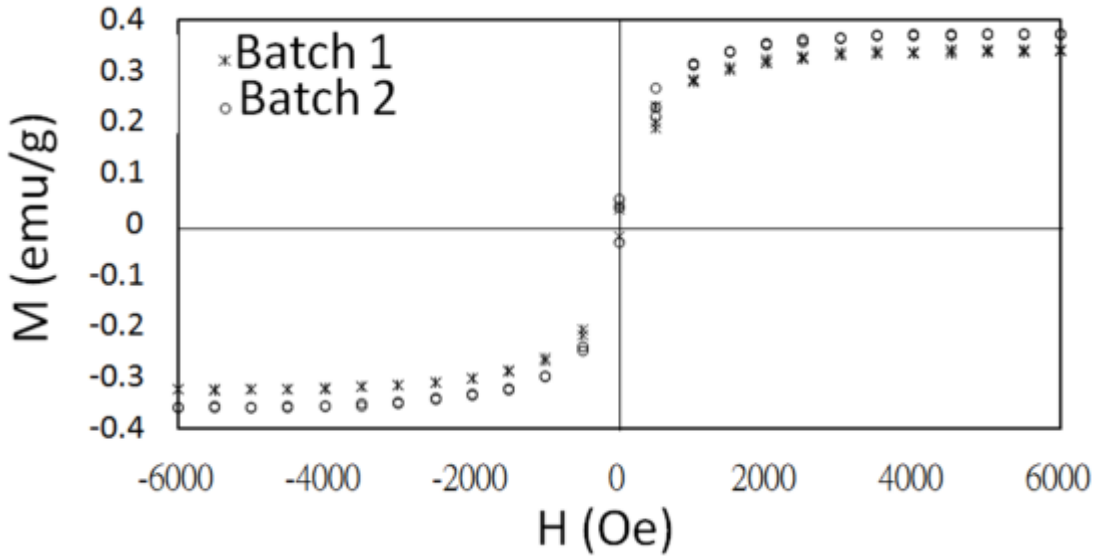

Figure S3. Hysteresis curve of two batches of anti-AFP reagent

2. The spectrum analysis of the measured signal

The spectrum of a particular measured signal, namely, the square shape of dried anti-AFP MNPs in the phantom test, is shown in Figure S4. It indicates the ultrasound excitation was performed at 5 MHz. The signal-to-noise ratio was approximately 60.

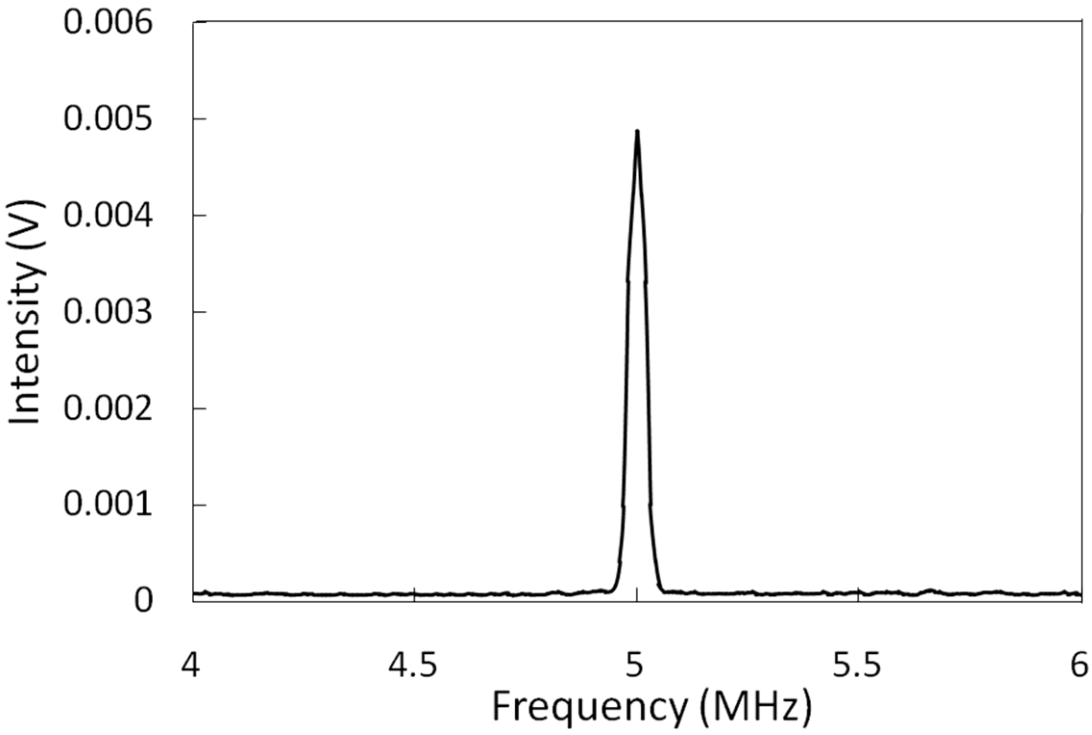

Figure S4. Spectrum of the measured signal

3. The mathematical theory of detection

The imaging utilizes an ultrasound focus with strong acoustic pressure to vibrate the magnetized samples. The pickup coils, as shown in Figure S5, detect signals as follows.

The magnetic field $\vec{H}(\vec{r})$ of the magnetized sample with a dipole placed at $\vec{r}$ is given as follows:

$$\vec{\mathrm{H}}(\vec{\mathrm{r}}) = \frac{1}{4\pi}\left[\frac{3\vec{\mathrm{r}}(\vec{\mathrm{m}}\cdot\vec{\mathrm{r}})}{|\vec{\mathrm{r}}|^5} - \frac{\vec{\mathrm{m}}}{|\vec{\mathrm{r}}|^3}\right] \quad \text{.....(S1)}$$

where $\vec{r}$ is the position vector of a point in space, and *m* is the magnetization of the sample.

If the position of this sample is varied over a small distance $\vec{\delta}(t)$, then a change of flux $\partial\vec{B}(t)$ that is induced at a point $\vec{r}$ in space can be defined as:

$$\partial\vec{\mathrm{B}}(\mathrm{t}) = \mu_0\vec{\delta}(\mathrm{t})\cdot\nabla\{\overrightarrow{\mathrm{H_z}}(\vec{\mathrm{r}})\} = \frac{3\mu_0\cdot\vec{\mathrm{m}}\cdot\vec{\mathrm{x}}\cdot|\vec{\delta}(\mathrm{t})|}{4\pi}\cdot\frac{\partial}{\partial \mathrm{z}}\left(\frac{\mathrm{z}}{|\vec{\mathrm{r}}|^5}\right) \quad \text{.....(S2)}$$

If we place a small coil at the origin then the voltage induced in it will be given by as follows:

$$\mathrm{v}(\mathrm{t}) = \sum_{\mathrm{PC}}\sum_{\mathrm{N_c}}\sum_{\mathrm{N_t}}\int_{\mathrm{A}}\left(\frac{\partial\vec{B}(\mathrm{t})}{\partial \mathrm{t}}\right)\cdot \mathrm{d}\vec{\mathrm{A}} \quad \text{.....(S3)}$$

where N_t is the number of turns, *A* denotes the area vector of a single turn, N_c is the number of coils, and PC is two element pickup coils.

In this work, the system sensitivity, $\partial\vec{B}(t)$,was approximately 87 pT, and the vibration amplitude, $\overrightarrow{\delta_z}(t)$, of MNPs distributed on phantom or animal tissue was reasonably assumed to be approximately half of the ultrasound wavelength of 0.1 mm. In addition to the minimum horizontal distance, $\vec{x}$, around 1.0 mm between the sample and the center of the pickup coil, the worst depth, $\vec{z}$, was approximately 1.0 cm for the *in vitro* test and 10.0 cm for the *in vivo* human test. Hence, for the *in vitro* and *in vivo* tests, the values of detectable minimum magnetization, *m*, were 7.26×10^{-8} and 7.25×10^{-3} $\mathrm{A\cdot m^2}$ from the detectable minimum MNPs of 2.9×10^{-15} and 2.9×10^{-10} mole, containing the detectable minimum iron amounts of $5.7\times10^{-7}$and 5.7×10^{-2} g. Further, to evaluate the weight and size of the detectable minimum liver tumors targeted by MNPs, the iron concentration and density of the liver tumors were obtained. The former was 107.5 ppm from the inductively-coupled-plasma (PE-SCIEX ELAN 6100 DRC, PerkinElmer Inc., USA) measurement of liver tumors at 8h postinjection. The latter

was assumed to be 1.05 g/cm^{3}based on other work.[S3] Hence, for the worst depths of 1.0 cm in the *in vitro* test and 10.0 cm in the *in vivo* human test, the weights and sizes of the detectable minimum liver tumors were approximately 5.34 mg and 532.9 g in weight, and 2.1 mm and 98.9 mm in diameter. The detection performance for distant tumors could be easily improved by the higher injection dose or the better system sensitivity than this work.

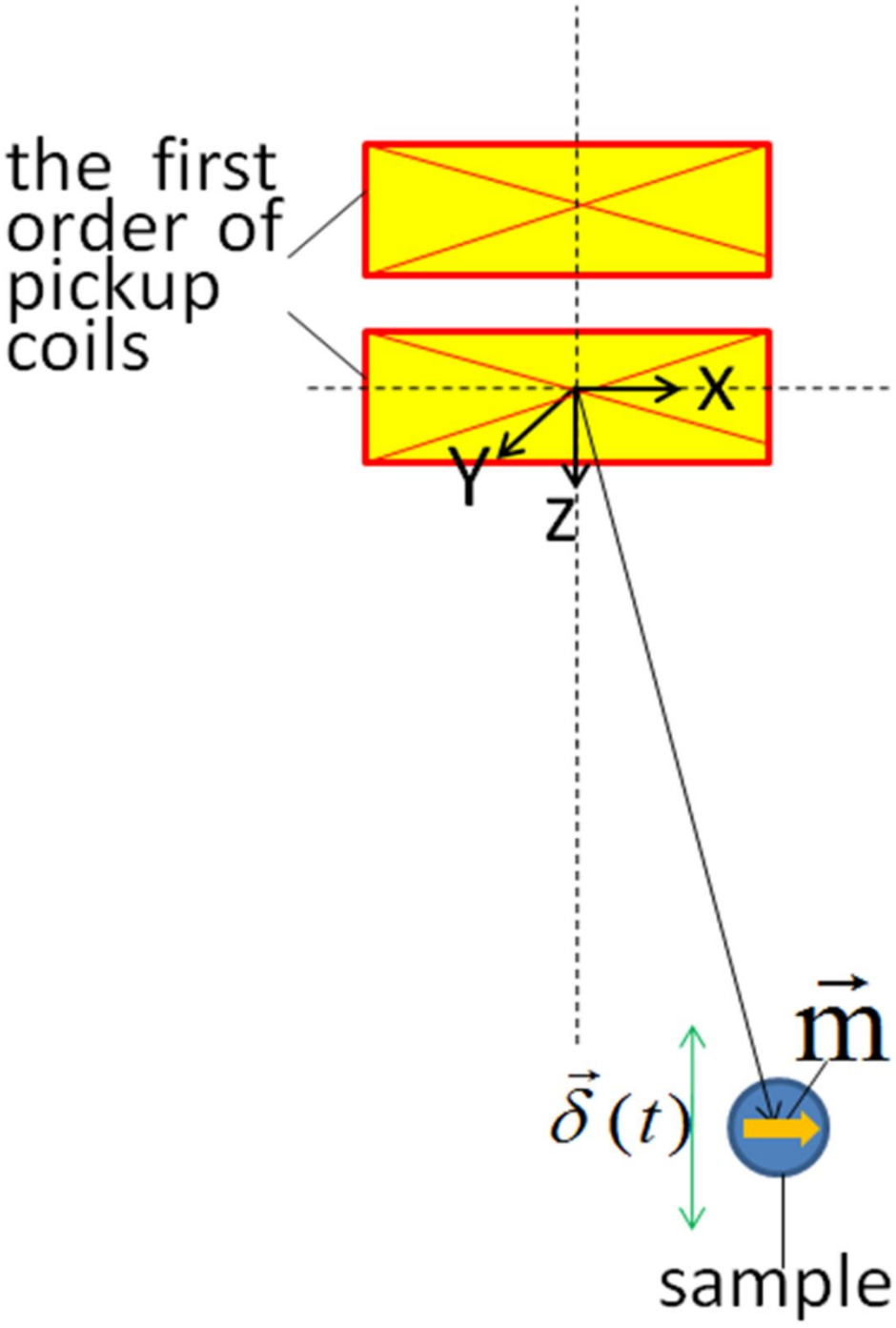

Figure S5. Detection of the pickup coils for the vibrated sample with a vibration amplitude $\vec{\delta}(t)$.

4. The construction of the image

The details of the image construction are described to explain the facticity of images as follows.

For example, a 0.1-mm-thickpiece of gauze was used with the distribution of dried anti-AFP MNPs that had approximately 60 μg Fe. The gauze had a square shape,1 cm long on aside, and was positioned at a depth of 15 mm from the upper surface of the phantom.

The probe of the ultrasound-motivated magnetic imaging scanned a 3 × 3 cm area. The probe scanned around the center of the anti-AFP MNP distribution. The path is indicated with lines composed of red dots in the illustrations of the phantom. An x–y step motor moved the probe at a speed of 1 mm/step. In each scanning step, the ultrasound focus from the ultrasound chips vibrated anti-AFP MNP distributions of the square shape at a depth of 15 mm from the upper surface of the phantom. The intensity variations along the scanning path were used to construct the red, square image of the 3 × 3 cm area. For example, the lower inset of Figure S6 shows a signal variation, marked with a blue solid line. That information was gathered by moving the probe along the scanning path, marked with a blue dotted line in the upper inset.

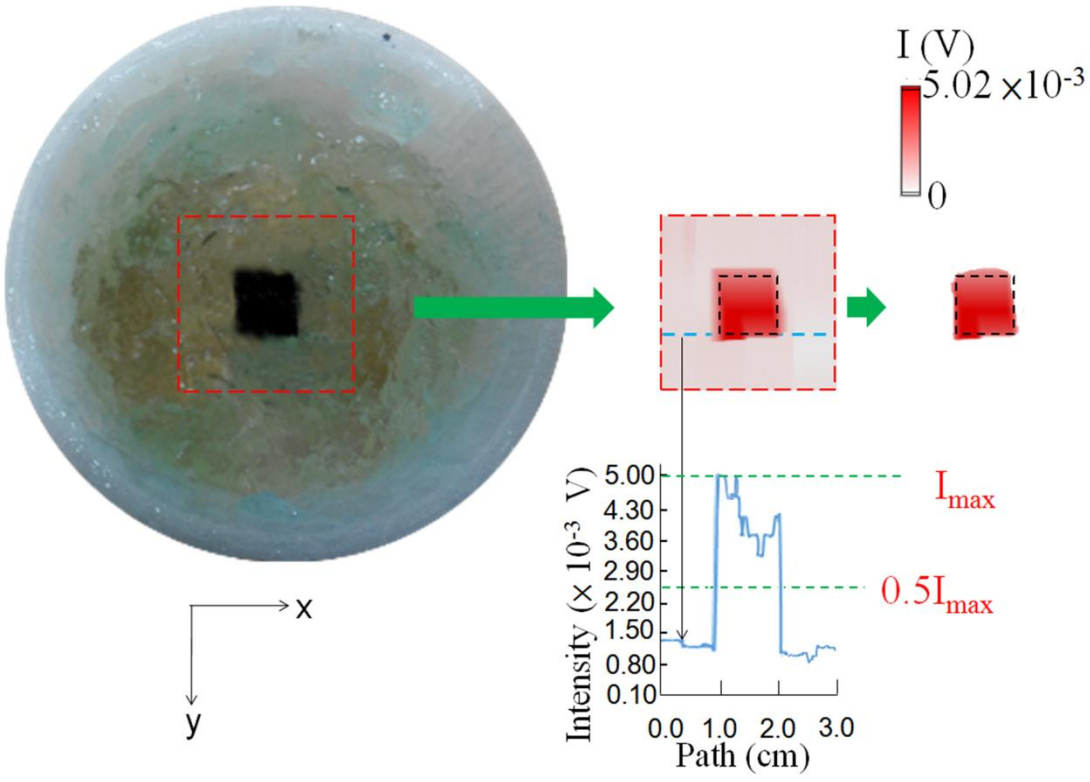

Figure S6. Scheme of magnetic image construction

In magnetology, the sensed magnetic signals are always distributed spherically from the magnetic source, as explained by the Biot–Savart law. Hence, a previous work[S4] obtained an optical image from an integrated charge-coupled device with a pickup coil, then consecutively and numerically utilized the 2D size of a MNP distribution in that optical image to filter the size of magnetic spots in magnetic images. The filtering method was that the pixels of each magnetic spot were interpreted as the real MNP distribution, and pixels' signals were retained if their magnetic intensities were larger than 50% of the maximum intensity of the magnetic spot. The spatial contour error between the red spot in the filtered magnetic image and the real distribution of MNPs in the optical image was within 3 mm. Therefore, for the magnetic image, a large square shape, marked by the red dotted line of 3 × 3 cm, was cut into a small shape by removing the signal lower than 50% I_{max}. This is indicated by the black dotted line of 1 × 1 cm in the upper inset of Figure S6.

6. References

(1) Yang, J.W.; Yang, H. C.; Yang, S.Y.; Horng, H.E.; Hung, J. C.; Chen, Y.C.; Hong, C.Y. Preparation and Properties of Superparamagnetic Nanoparticles with Narrow Size Distribution and Biocompatible. *J. Magn. Magn. Mater.***2004**, 283, 210–4.

(2)Liu, W.; Ming, Z.; Kong,L. Estimation of the Size Distribution of Magnetic Nanoparticles Using Modified Magnetization Curves.*Meas. Sci. Technol.***2009**, 20, 125802.

(3) Jensen,J.H.;Chandra, R.Theory of Nonexponential NMR Signal Decay in Liver with Iron Overload or Superparamagnetic Iron Oxide Particles.*Magn. Reson. Med.***2002**, 47, 1131–1138.

(4) Chieh, J. J.; Huang, K.W.; Lee, Y. Y.; Wei, W. C. Dual-Imaging Model of SQUID Biosusceptometry for Locating Tumors Targeted Using Magnetic Nanoparticles. *J. Nanobiotechnol.***2015**, 13, 11.